

## MULTIDIMENSIONAL RELAXATION APPROXIMATIONS FOR HYPERBOLIC SYSTEMS OF CONSERVATION LAWS <sup>\*1)</sup>

Mohammed Seaid

(Universität Kaiserslautern Fachbereich Mathematik, 67663 Kaiserslautern, Germany

Email: seaid@mathematik.uni-kl.de)

### Abstract

We construct and implement a non-oscillatory relaxation scheme for multidimensional hyperbolic systems of conservation laws. The method transforms the nonlinear hyperbolic system to a semilinear model with a relaxation source term and linear characteristics which can be solved numerically without using either Riemann solver or linear iterations. To discretize the relaxation system we consider a high-resolution reconstruction in space and a TVD Runge-Kutta time integration. Detailed formulation of the scheme is given for problems in three space dimensions and numerical experiments are implemented in both scalar and system cases to show the effectiveness of the method.

*Mathematics subject classification:* 35L60, 35L65, 82B40, 65M20, 74S10, 65L06.

*Key words:* Multidimensional hyperbolic systems, Relaxation methods, Non-oscillatory reconstructions, Asymptotic-preserving schemes.

### 1. Introduction

In this paper we are interested in solving numerically the multidimensional hyperbolic system of conservation laws

$$\frac{\partial \mathbf{U}}{\partial t} + \frac{\partial \mathbf{F}(\mathbf{U})}{\partial x} + \frac{\partial \mathbf{G}(\mathbf{U})}{\partial y} + \frac{\partial \mathbf{H}(\mathbf{U})}{\partial z} = \mathbf{0}, \quad t > 0, \quad (x, y, z) \in \mathbb{R}^3, \quad (1.1a)$$

$$\mathbf{U}(t = 0, x, y, z) = \mathbf{U}_0(x, y, z), \quad (1.1b)$$

where  $\mathbf{U}(t, x, y, z) \in \mathbb{R}^N$  is a vector of conserved quantities;  $\mathbf{F}(\mathbf{U}) \in \mathbb{R}^N$ ,  $\mathbf{G}(\mathbf{U}) \in \mathbb{R}^N$  and  $\mathbf{H}(\mathbf{U}) \in \mathbb{R}^N$  are nonlinear flux functions; and  $\mathbf{U}_0 \in \mathbb{R}^N$  is given initial data. We assume that the Jacobian matrices  $\partial \mathbf{F} / \partial \mathbf{U}$ ,  $\partial \mathbf{G} / \partial \mathbf{U}$  and  $\partial \mathbf{H} / \partial \mathbf{U}$  are diagonalizable with real eigenvalues  $\{\lambda_1, \dots, \lambda_N\}$ ,  $\{\mu_1, \dots, \mu_N\}$  and  $\{\xi_1, \dots, \xi_N\}$ , respectively.

The relaxation system proposed in [7] and considered in this paper reads

$$\frac{\partial \mathbf{U}}{\partial t} + \frac{\partial \mathbf{V}}{\partial x} + \frac{\partial \mathbf{W}}{\partial y} + \frac{\partial \mathbf{Z}}{\partial z} = \mathbf{0}, \quad (1.2a)$$

$$\frac{\partial \mathbf{V}}{\partial t} + \mathbf{A} \frac{\partial \mathbf{U}}{\partial x} = -\frac{1}{\varepsilon} (\mathbf{V} - \mathbf{F}(\mathbf{U})), \quad (1.2b)$$

$$\frac{\partial \mathbf{W}}{\partial t} + \mathbf{B} \frac{\partial \mathbf{U}}{\partial y} = -\frac{1}{\varepsilon} (\mathbf{W} - \mathbf{G}(\mathbf{U})), \quad (1.2c)$$

$$\frac{\partial \mathbf{Z}}{\partial t} + \mathbf{C} \frac{\partial \mathbf{U}}{\partial z} = -\frac{1}{\varepsilon} (\mathbf{Z} - \mathbf{H}(\mathbf{U})), \quad (1.2d)$$

---

\* Received October 10, 2005; final revised March 7, 2006; accepted April 20, 2006.

<sup>1)</sup> This work was supported by the German research foundation DFG under grant KL 1105/9-1.

where  $\mathbf{V} \in \mathbb{R}^N$ ,  $\mathbf{W} \in \mathbb{R}^N$  and  $\mathbf{Z} \in \mathbb{R}^N$  are relaxation variables;  $\mathbf{A} = \text{diag}\{A_1, \dots, A_N\}$ ,  $\mathbf{B} = \text{diag}\{B_1, \dots, B_N\}$  and  $\mathbf{C} = \text{diag}\{C_1, \dots, C_N\}$  are positive diagonal matrices; and  $\varepsilon > 0$  is the relaxation time. The relaxation system (1.2) has a typical semilinear structure with linear characteristic variables defined by

$$\mathbf{V} \pm \sqrt{\mathbf{A}}\mathbf{U}, \quad \mathbf{W} \pm \sqrt{\mathbf{B}}\mathbf{U} \quad \text{and} \quad \mathbf{Z} \pm \sqrt{\mathbf{C}}\mathbf{U}. \quad (1.3)$$

Formally, in the zero relaxation limit  $\varepsilon \rightarrow 0$ , we recover the original system (1.1) provided the subcharacteristic condition [7, 11, 8],

$$\frac{\lambda_\nu^2}{A_\nu} + \frac{\mu_\nu^2}{B_\nu} + \frac{\xi_\nu^2}{C_\nu} \leq 1, \quad \forall \nu = 1, \dots, N, \quad (1.4)$$

holds in (1.2). Note that if we project the relaxation variables into the local equilibrium

$$\mathbf{V} = \mathbf{F}(\mathbf{U}), \quad \mathbf{W} = \mathbf{G}(\mathbf{U}) \quad \text{and} \quad \mathbf{Z} = \mathbf{H}(\mathbf{U}), \quad (1.5)$$

then the first equation of (1.2) reduces to the original conservation laws (1.1). Further references on the analysis and convergence of relaxation methods can be found in [19, 20] among others.

Our aim in this paper is to reconstruct high order relaxation schemes for the hyperbolic systems (1.1) in multi-space dimensions. The central key for such reconstruction is the combination of Weighted Essentially Non-Oscillatory (WENO) polynomials for the space discretization and asymptotic-preserving implicit-explicit (IMEX) methods for the time integration. Although we concentrate on a third-order reconstruction, the formalism presented here can readily be applied to develop relaxation methods with arbitrary order of accuracy. It is worthwhile to mention that WENO schemes of order between 7 and 11 can be found in the literature, compare [3] for details. We also should mention that central schemes [6] and non-uniform mesh methods [18] offer useful numerical tools for solving multi-dimensional hyperbolic systems of conservation laws. However, all these methods solve the relaxed original problem (1.1) instead of the relaxation system (1.2). In many practical applications one may also be interested in the transient regimes before the equilibrium. For instance, there is strong links between relaxation methods and kinetic or lattice Boltzmann schemes used in the frame of Boltzmann equation (as a simple case, the BGK model which offers a similar structure as the one we referred to as relaxation system (1.2) with  $\varepsilon$  denotes the Knudsen number). It is well known that, by keeping the Knudsen number small one can derive inviscid Euler problems from the kinetic equation. However, it is a challenging problem to construct consistent space and time discretization of the transient equations that preserve the asymptotic limit and converge to the correct numerical solution of the limit equations as the Knudsen number goes to zero. Therefore, one of the purposes of our work was to combine in a formal way a high order space and time discretizations in order to construct a numerical method that works for both small and large relaxation rates  $\varepsilon$ .

The design of high order relaxation schemes has been partially addressed by other authors in [13, 10], however, in those references the formulations and numerical results are given only for the one-dimensional problems. Extension to the two-dimensional hyperbolic systems was recently discussed in [14, 5] along with a comparison between relaxed schemes ( $\varepsilon = 0$ ) and the well-established central methods. Relaxation methods were also used in [15] for the shallow water equations in one and two space dimensions and in [16] for the two-dimensional Riemann problems in gas dynamics. To our knowledge, this is the first time that multi-dimensional hyperbolic systems of conservation laws are approximated by relaxation techniques. To demonstrate the basic algorithms, and show that it can adapt to multi-dimensional features of a solution,

we have implemented a third-order relaxation scheme to solve the scalar Burgers' equation and the Euler system of inviscid gas dynamics.

### 2. Third-order Relaxation Method

To develop a relaxation scheme for the system (1.2), it is convenient to treat the spatial and temporal discretizations separately using the method of lines.

#### 2.1. The semi-discrete approximation

We divide the spatial domain into cells  $I_{i,j,k} = [x_{i-\frac{1}{2}}, x_{i+\frac{1}{2}}] \times [y_{j-\frac{1}{2}}, y_{j+\frac{1}{2}}] \times [z_{k-\frac{1}{2}}, z_{k+\frac{1}{2}}]$  with uniform sizes  $\Delta x$ ,  $\Delta y$  and  $\Delta z$  and centered at  $(x_i = i\Delta x, y_j = j\Delta y, z_k = k\Delta z)$ . We use the notations  $\mathbf{U}_{i\pm\frac{1}{2},j,k}(t) = \mathbf{U}(t, x_{i\pm\frac{1}{2}}, y_j, z_k)$ ,  $\mathbf{U}_{i,j\pm\frac{1}{2},k}(t) = \mathbf{U}(t, x_i, y_{j\pm\frac{1}{2}}, z_k)$ ,  $\mathbf{U}_{i,j,k\pm\frac{1}{2}}(t) = \mathbf{U}(t, x_i, y_j, z_{k\pm\frac{1}{2}})$  and

$$\mathbf{U}_{i,j,k}(t) = \frac{1}{\Delta x} \frac{1}{\Delta y} \frac{1}{\Delta z} \int_{x_{i-\frac{1}{2}}}^{x_{i+\frac{1}{2}}} \int_{y_{j-\frac{1}{2}}}^{y_{j+\frac{1}{2}}} \int_{z_{k-\frac{1}{2}}}^{z_{k+\frac{1}{2}}} \mathbf{U}(t, x, y, z) dx dy dz,$$

to denote the point-values and the approximate cell-average of the function  $\mathbf{U}$  at  $(t, x_{i\pm\frac{1}{2}}, y_j, z_k)$ ,  $(t, x_i, y_{j\pm\frac{1}{2}}, z_k)$ ,  $(t, x_i, y_j, z_{k\pm\frac{1}{2}})$ , and  $(t, x_i, y_j, z_k)$ , respectively. We also use the following difference notation

$$\begin{aligned} \mathcal{D}_x \mathbf{U}_{i,j,k} &= \frac{\mathbf{U}_{i+\frac{1}{2},j,k} - \mathbf{U}_{i-\frac{1}{2},j,k}}{\Delta x}, & \mathcal{D}_y \mathbf{U}_{i,j,k} &= \frac{\mathbf{U}_{i,j+\frac{1}{2},k} - \mathbf{U}_{i,j-\frac{1}{2},k}}{\Delta y}, \\ \mathcal{D}_z \mathbf{U}_{i,j,k} &= \frac{\mathbf{U}_{i,j,k+\frac{1}{2}} - \mathbf{U}_{i,j,k-\frac{1}{2}}}{\Delta z}. \end{aligned} \tag{2.1}$$

Then, the space discretization of (1.2) reads

$$\frac{d\mathbf{U}_{i,j,k}}{dt} + \mathcal{D}_x \mathbf{V}_{i,j,k} + \mathcal{D}_y \mathbf{W}_{i,j,k} + \mathcal{D}_z \mathbf{Z}_{i,j,k} = \mathbf{0}, \tag{2.2a}$$

$$\frac{d\mathbf{V}_{i,j,k}}{dt} + \mathbf{A} \mathcal{D}_x \mathbf{U}_{i,j,k} = -\frac{1}{\varepsilon} \left( \mathbf{V}_{i,j,k} - \mathbf{F}(\mathbf{U})_{i,j,k} \right), \tag{2.2b}$$

$$\frac{d\mathbf{W}_{i,j,k}}{dt} + \mathbf{B} \mathcal{D}_y \mathbf{U}_{i,j,k} = -\frac{1}{\varepsilon} \left( \mathbf{W}_{i,j,k} - \mathbf{G}(\mathbf{U})_{i,j,k} \right), \tag{2.2c}$$

$$\frac{d\mathbf{Z}_{i,j,k}}{dt} + \mathbf{C} \mathcal{D}_z \mathbf{U}_{i,j,k} = -\frac{1}{\varepsilon} \left( \mathbf{Z}_{i,j,k} - \mathbf{H}(\mathbf{U})_{i,j,k} \right), \tag{2.2d}$$

The  $\nu$ -th component ( $\nu = 1, \dots, N$ ) of approximate solution is reconstructed by a piecewise polynomial over the gridpoints as

$$U_\nu(x, y, z, t) = \sum_{i,j,k} \mathcal{P}_{i,j,k}(x, y, z; \mathbf{U}) \chi_{i,j,k}(x, y, z), \tag{2.3}$$

where  $\chi_{i,j,k}$ 's are the characteristic functions in the cell  $I_{i,j,k}$ . The polynomials  $\mathcal{P}_{i,j,k}$  are defined in  $I_{i,j,k}$  and reconstructed "direction by direction" as

$$\mathcal{P}_{i,j,k}(x, y, z; \mathbf{U}) = \mathcal{P}_i(x, y, z; \mathbf{U}) + \mathcal{P}_j(x, y, z; \mathbf{U}) + \mathcal{P}_k(x, y, z; \mathbf{U}).$$

For simplicity in presentation, the subscript  $\nu$  will be omitted in (2.3). The degree of the polynomials  $\mathcal{P}_{i,j,k}$  is determined by the required order of accuracy of the method. In this paper

we consider the third-order WENO reconstruction from [17]. Other WENO reconstructions of order higher than three are also presented in [17], their implementation in the relaxation framework can be formulated following the same arguments discussed in this paper. In the following we formulate the  $x$ -direction polynomial  $\mathcal{P}_i(x, y, z; \mathbf{U})$ , the formulation of  $\mathcal{P}_j(x, y, z; \mathbf{U})$  and  $\mathcal{P}_k(x, y, z; \mathbf{U})$  can be done analogously. Hence

$$\mathcal{P}_i(x, y, z; \mathbf{U}) = \omega_{-1}P_{-1}(x, y, z) + \omega_0P_0(x, y, z) + \omega_{+1}P_{+1}(x, y, z),$$

where the weights  $\omega_l, l \in \{-1, 0, +1\}$  are defined as

$$\omega_l = \frac{\alpha_l}{\sum_m \alpha_m}, \quad l, m \in \{-1, 0, +1\}, \quad \alpha_l = \frac{c_l}{(IS_l)^2}, \quad c_{-1} = c_{+1} = \frac{1}{4}, \quad c_0 = \frac{1}{2}.$$

Note that the normalizing factor  $\sum_m \alpha_m$  is used here to guarantee  $\sum_l \omega_l = 1$ . The smoothness indicators  $IS_l$  and the polynomials  $P_l(x, y, z)$  are given by

$$\begin{aligned} IS_{-1} &= (U_{i,j,k} - U_{i-1,j,k})^2, & IS_{+1} &= (U_{i+1,j,k} - U_{i,j,k})^2, \\ IS_0 &= \frac{13}{3}(U_{i+1,j,k} - 2U_{i,j,k} + U_{i-1,j,k})^2 + \frac{1}{4}(U_{i+1,j,k} - U_{i-1,j,k})^2, \\ P_{-1}(x) &= U_{i,j,k} + \frac{U_{i,j,k} - U_{i-1,j,k}}{\Delta x}(x - x_i), & P_{+1}(x) &= U_{i,j,k} + \frac{U_{i+1,j,k} - U_{i,j,k}}{\Delta x}(x - x_i), \\ P_0(x) &= U_{i,j,k} - \frac{1}{12}(U_{i+1,j,k} - 2U_{i,j,k} + U_{i-1,j,k}) \\ &\quad - \frac{1}{12}(U_{i,j+1,k} - 2U_{i,j,k} + U_{i,j-1,k}) - \frac{1}{12}(U_{i,j+1,k} - 2U_{i,j,k} + U_{i,j,k-1}) \\ &\quad + \frac{U_{i+1,j,k} - U_{i-1,j,k}}{2(\Delta x)}(x - x_i) + \frac{(U_{i+1,j,k} - 2U_{i,j,k} + U_{i-1,j,k})}{(\Delta x)^2}(x - x_i)^2. \end{aligned}$$

We can now discretize the characteristic variables (1.3) as follows

$$(V \pm \sqrt{A_\nu}U)_{i+\frac{1}{2},j,k} = \mathcal{P}_i(x_{i+\frac{1}{2}}, y_j, z_k; \mathbf{V} \pm \sqrt{\mathbf{A}}\mathbf{U}), \tag{2.4a}$$

$$(W \pm \sqrt{B_\nu}U)_{i,j+\frac{1}{2},k} = \mathcal{P}_j(x_i, y_{j+\frac{1}{2}}, z_k; \mathbf{W} \pm \sqrt{\mathbf{B}}\mathbf{U}), \tag{2.4b}$$

$$(Z \pm \sqrt{C_\nu}U)_{i,j,k+\frac{1}{2}} = \mathcal{P}_k(x_i, y_j, z_{k+\frac{1}{2}}; \mathbf{Z} \pm \sqrt{\mathbf{C}}\mathbf{U}). \tag{2.4c}$$

Recall that  $U, V, W, Z, A_\nu, B_\nu$  and  $C_\nu$  are the  $\nu$ -th ( $\nu = 1, \dots, N$ ) components of  $\mathbf{U}, \mathbf{V}, \mathbf{W}, \mathbf{Z}, \mathbf{A}, \mathbf{B}$  and  $\mathbf{C}$ , respectively. Solving (2.4) for the unknowns  $U_{i+\frac{1}{2},j,k}, V_{i+\frac{1}{2},j,k}, U_{i,j+\frac{1}{2},k}, W_{i,j+\frac{1}{2},k}, U_{i,j,k+\frac{1}{2}}$  and  $Z_{i,j,k+\frac{1}{2}}$  gives

$$\begin{aligned} U_{i+\frac{1}{2},j,k} &= \frac{1}{2\sqrt{A_\nu}} \left( \mathcal{P}_i(x_{i+\frac{1}{2}}, y_j, z_k; \mathbf{V} + \sqrt{\mathbf{A}}\mathbf{U}) - \mathcal{P}_{i+1}(x_{i+\frac{1}{2}}, y_j, z_k; \mathbf{V} - \sqrt{\mathbf{A}}\mathbf{U}) \right), \\ V_{i+\frac{1}{2},j,k} &= \frac{1}{2} \left( \mathcal{P}_i(x_{i+\frac{1}{2}}, y_j, z_k; \mathbf{V} + \sqrt{\mathbf{A}}\mathbf{U}) + \mathcal{P}_{i+1}(x_{i+\frac{1}{2}}, y_j, z_k; \mathbf{V} - \sqrt{\mathbf{A}}\mathbf{U}) \right), \\ U_{i,j+\frac{1}{2},k} &= \frac{1}{2\sqrt{B_\nu}} \left( \mathcal{P}_j(x_i, y_{j+\frac{1}{2}}, z_k; \mathbf{W} + \sqrt{\mathbf{B}}\mathbf{U}) - \mathcal{P}_{j+1}(x_i, y_{j+\frac{1}{2}}, z_k; \mathbf{W} - \sqrt{\mathbf{B}}\mathbf{U}) \right), \\ W_{i,j+\frac{1}{2},k} &= \frac{1}{2} \left( \mathcal{P}_j(x_i, y_{j+\frac{1}{2}}, z_k; \mathbf{W} + \sqrt{\mathbf{B}}\mathbf{U}) + \mathcal{P}_{j+1}(x_i, y_{j+\frac{1}{2}}, z_k; \mathbf{W} - \sqrt{\mathbf{B}}\mathbf{U}) \right), \\ U_{i,j,k+\frac{1}{2}} &= \frac{1}{2\sqrt{C_\nu}} \left( \mathcal{P}_k(x_i, y_j, z_{k+\frac{1}{2}}; \mathbf{Z} + \sqrt{\mathbf{C}}\mathbf{U}) - \mathcal{P}_{k+1}(x_i, y_j, z_{k+\frac{1}{2}}; \mathbf{Z} - \sqrt{\mathbf{C}}\mathbf{U}) \right), \\ Z_{i,j,k+\frac{1}{2}} &= \frac{1}{2} \left( \mathcal{P}_k(x_i, y_j, z_{k+\frac{1}{2}}; \mathbf{Z} + \sqrt{\mathbf{C}}\mathbf{U}) + \mathcal{P}_{k+1}(x_i, y_j, z_{k+\frac{1}{2}}; \mathbf{Z} - \sqrt{\mathbf{C}}\mathbf{U}) \right). \end{aligned}$$

Therefore, we obtain the following expressions for the numerical fluxes in the semi-discrete equations (2.2)

$$\begin{aligned}
U_{i+\frac{1}{2},j,k} &= \frac{U_{i,j,k} + U_{i+1,j,k}}{2} - \frac{V_{i+1,j,k} - V_{i,j,k}}{2\sqrt{A_\nu}} + \frac{\sigma_{i,j,k}^{x,+} + \sigma_{i+1,j,k}^{x,-}}{4\sqrt{A_\nu}}, \\
V_{i+\frac{1}{2},j,k} &= \frac{V_{i,j,k} + V_{i+1,j,k}}{2} - \sqrt{A_\nu} \frac{U_{i+1,j,k} - U_{i,j,k}}{2} + \frac{\sigma_{i,j,k}^{x,+} - \sigma_{i+1,j,k}^{x,-}}{4}, \\
U_{i,j+\frac{1}{2},k} &= \frac{U_{i,j,k} + U_{i,j+1,k}}{2} - \frac{W_{i,j+1,k} - W_{i,j,k}}{2\sqrt{B_\nu}} + \frac{\sigma_{i,j,k}^{y,+} + \sigma_{i,j+1,k}^{y,-}}{4\sqrt{B_\nu}}, \\
W_{i,j+\frac{1}{2},k} &= \frac{W_{i,j,k} + W_{i,j+1,k}}{2} - \sqrt{B_\nu} \frac{U_{i,j+1,k} - U_{i,j,k}}{2} + \frac{\sigma_{i,j,k}^{y,+} - \sigma_{i,j+1,k}^{y,-}}{4}, \\
U_{i,j,k+\frac{1}{2}} &= \frac{U_{i,j,k} + U_{i,j,k+1}}{2} - \frac{Z_{i,j,k+1} - Z_{i,j,k}}{2\sqrt{C_\nu}} + \frac{\sigma_{i,j,k}^{z,+} + \sigma_{i,j,k+1}^{z,-}}{4\sqrt{C_\nu}}, \\
Z_{i,j,k+\frac{1}{2}} &= \frac{Z_{i,j,k} + Z_{i,j,k+1}}{2} - \sqrt{C_\nu} \frac{U_{i,j,k+1} - U_{i,j,k}}{2} + \frac{\sigma_{i,j,k}^{z,+} - \sigma_{i,j,k+1}^{z,-}}{4},
\end{aligned}$$

where  $\sigma_{i,j,k}^{x,\pm}$ ,  $\sigma_{i,j,k}^{y,\pm}$  and  $\sigma_{i,j,k}^{z,\pm}$  are the slopes of  $\mathbf{V} \pm \sqrt{A_\nu}\mathbf{U}$ ,  $\mathbf{W} \pm \sqrt{B_\nu}\mathbf{U}$  and  $\mathbf{Z} \pm \sqrt{C_\nu}\mathbf{U}$  on the cell  $I_{i,j,k}$ , respectively. The value of  $\sigma_{i,j,k}^{x,\pm}$  is defined by

$$\begin{aligned}
\sigma_{i,j,k}^{x,\pm} &= \omega_{-1}^\pm \left( (V \pm \sqrt{A_\nu}U)_{i,j,k} - (V \pm \sqrt{A_\nu}U)_{i-1,j,k} \right) \\
&\quad + \frac{\omega_0^\pm}{2} \left( (V \pm \sqrt{A_\nu}U)_{i+1,j,k} - (V \pm \sqrt{A_\nu}U)_{i-1,j,k} \right) \\
&\quad + \frac{\omega_0^\pm}{3} \left( (V \pm \sqrt{A_\nu}U)_{i+1,j,k} - 2(V \pm \sqrt{A_\nu}U)_{i,j,k} + (V \pm \sqrt{A_\nu}U)_{i-1,j,k} \right) \\
&\quad - \frac{\omega_0^\pm}{9} \left( (V \pm \sqrt{A_\nu}U)_{i,j+1,k} - 2(V \pm \sqrt{A_\nu}U)_{i,j,k} + (V \pm \sqrt{A_\nu}U)_{i,j-1,k} \right) \\
&\quad - \frac{\omega_0^\pm}{9} \left( (V \pm \sqrt{A_\nu}U)_{i,j,k+1} - 2(V \pm \sqrt{A_\nu}U)_{i,j,k} + (V \pm \sqrt{A_\nu}U)_{i,j,k-1} \right) \\
&\quad + \omega_{+1}^\pm \left( (V \pm \sqrt{A_\nu}U)_{i+1,j,k} - (V \pm \sqrt{A_\nu}U)_{i,j,k} \right).
\end{aligned}$$

The values  $\sigma_{i,j,k}^{y,\pm}$  and  $\sigma_{i,j,k}^{z,\pm}$  are defined similarly. The weight parameters  $\omega_{-1}^\pm$ ,  $\omega_0^\pm$  and  $\omega_{+1}^\pm$  for  $\sigma_{i,j}^{x,\pm}$  are given by

$$\begin{aligned}
\omega_l^\pm &= \frac{\alpha_l^\pm}{\sum_m \alpha_m^\pm}, \quad l, m \in \{-1, 0, +1\}, \quad \alpha_l^\pm = \frac{c_l}{(IS_l^\pm)^2}, \quad c_{-1} = c_{+1} = \frac{1}{4}, \quad c_0 = \frac{1}{2}, \\
IS_{-1}^\pm &= \left( (V \pm \sqrt{A_\nu}U)_{i,j,k} - (V \pm \sqrt{A_\nu}U)_{i-1,j,k} \right)^2, \\
IS_0^\pm &= \frac{13}{3} \left( (V \pm \sqrt{A_\nu}U)_{i+1,j,k} - 2(V \pm \sqrt{A_\nu}U)_{i,j,k} + (V \pm \sqrt{A_\nu}U)_{i-1,j,k} \right)^2 \\
&\quad + \frac{1}{4} \left( (V \pm \sqrt{A_\nu}U)_{i+1,j,k} - (V \pm \sqrt{A_\nu}U)_{i-1,j,k} \right)^2, \\
IS_{+1}^\pm &= \left( (V \pm \sqrt{A_\nu}U)_{i+1,j,k} - (V \pm \sqrt{A_\nu}U)_{i,j,k} \right)^2.
\end{aligned}$$

The corresponding weight parameters for  $\sigma_{i,j,k}^{y,\pm}$  or  $\sigma_{i,j,k}^{z,\pm}$  are obtained by changing  $V \pm \sqrt{A_\nu}U$  to  $W \pm \sqrt{B_\nu}U$  or  $Z \pm \sqrt{C_\nu}U$  in the above formulas and differentiating respect to  $y$ -direction or

$z$ -direction, respectively. We would like to point out that in this higher order scheme we approximate  $\mathbf{F}(\mathbf{U})_{i,j,k}$ ,  $\mathbf{G}(\mathbf{U})_{i,j,k}$  and  $\mathbf{H}(\mathbf{U})_{i,j,k}$  in (2.2) using the fourth-order Simpson quadrature rule as opposed to the Midpoint Rule which was used in the first and second order reconstructions in [7].

**2.2. The fully-discrete approximation**

The semi-discrete system (2.2) can be rewritten as a system of ordinary differential equations of form

$$\frac{d\mathbf{Y}}{dt} = \Phi(\mathbf{Y}) - \frac{1}{\varepsilon}\Psi(\mathbf{Y}), \tag{2.5}$$

where  $\mathbf{Y} = [\mathbf{U}_{i,j,k}, \mathbf{V}_{i,j,k}, \mathbf{W}_{i,j,k}, \mathbf{Z}_{i,j,k}]^T$  and the time-dependent vector functions  $\Psi$  and  $\Phi$  are given by

$$\Psi(\mathbf{Y}) = \begin{pmatrix} \mathbf{0} \\ \mathbf{V}_{i,j,k} - \mathbf{F}(\mathbf{U})_{i,j,k} \\ \mathbf{W}_{i,j,k} - \mathbf{G}(\mathbf{U})_{i,j,k} \\ \mathbf{Z}_{i,j,k} - \mathbf{H}(\mathbf{U})_{i,j,k} \end{pmatrix}, \quad \Phi(\mathbf{Y}) = \begin{pmatrix} -\mathcal{D}_x \mathbf{V}_{i,j,k} - \mathcal{D}_y \mathbf{W}_{i,j,k} - \mathcal{D}_z \mathbf{Z}_{i,j,k} \\ -\mathbf{A} \mathcal{D}_x \mathbf{U}_{i,j,k} \\ -\mathbf{B} \mathcal{D}_y \mathbf{W}_{i,j,k} \\ -\mathbf{C} \mathcal{D}_z \mathbf{Z}_{i,j,k} \end{pmatrix}.$$

When  $\varepsilon \rightarrow 0$ , the equations (2.5) become highly stiff and any explicit treatment of the right hand side in (2.5) requires extremely small time stepsizes. This fact might restrict any long term computation in (1.2). On the other hand, integrating the equations (2.5) by implicit scheme, either linear or nonlinear algebraic equations have to be solved at every time step of the computational process. To find solutions of such systems is computationally very demanding. In this paper we consider an alternative approach based on implicit-explicit (IMEX) Runge-Kutta splitting. The non stiff stage of the splitting for  $\Phi$  is treated by an explicit Runge-Kutta scheme, while the stiff stage for  $\Psi$  is approximated by a diagonally implicit Runge-Kutta (DIRK) scheme. Compare [2, 12] for more details.

Let  $\Delta t$  be the time step and  $\mathbf{Y}^n$  denotes the approximate solution at  $t = n\Delta t$ . We formulate the IMEX scheme for the system (2.5) as

$$\begin{aligned} \mathbf{K}_l &= \mathbf{Y}^n + \Delta t \sum_{m=1}^{l-1} \tilde{a}_{lm} \Phi(\mathbf{K}_m) - \frac{\Delta t}{\varepsilon} \sum_{m=1}^s a_{lm} \Psi(\mathbf{K}_m), \quad l = 1, 2, \dots, s, \\ \mathbf{Y}^{n+1} &= \mathbf{Y}^n + \Delta t \sum_{l=1}^s \tilde{b}_l \Phi(\mathbf{K}_l) - \frac{\Delta t}{\varepsilon} \sum_{l=1}^s b_l \Psi(\mathbf{K}_l). \end{aligned} \tag{2.6}$$

The  $s \times s$  matrices  $\tilde{A} = (\tilde{a}_{lm})$ ,  $\tilde{a}_{lm} = 0$  for  $m \geq l$  and  $A = (a_{lm})$  are chosen such that the resulting scheme is explicit in  $\Phi$ , and implicit in  $\Psi$ . The  $s$ -vectors  $\tilde{b}$  and  $b$  are the canonical coefficients which characterize the IMEX  $s$ -stage Runge-Kutta scheme [12]. They can be given by the standard double *tableau* in Butcher notation,

$$\begin{array}{c|c} \tilde{c} & \tilde{A} \\ \hline & b^T \end{array} \qquad \begin{array}{c|c} c & A \\ \hline & b^T \end{array}$$

Here,  $\tilde{c}$  and  $c$  are  $s$ -vectors used in non autonomous cases. The implementation of the IMEX algorithm to solve (2.5) can be carried out in the following steps:

1. For  $l = 1, \dots, s$ ,
  - (a) Evaluate  $\mathbf{K}_l^*$  as:  $\mathbf{K}_l^* = \mathbf{Y}^n + \Delta t \sum_{m=1}^{l-2} \tilde{a}_{lm} \Phi(\mathbf{K}_m) + \Delta t \tilde{a}_{ll-1} \Phi(\mathbf{K}_{l-1})$ .
  - (b) Solve for  $\mathbf{K}_l$ :  $\mathbf{K}_l = \mathbf{K}_l^* - \frac{\Delta t}{\varepsilon} \sum_{m=1}^{l-1} a_{lm} \Psi(\mathbf{K}_m) - \frac{\Delta t}{\varepsilon} a_{ll} \Psi(\mathbf{K}_l)$ .
2. Update  $\mathbf{Y}^{n+1}$  as:  $\mathbf{Y}^{n+1} = \mathbf{Y}^n + \Delta t \sum_{l=1}^s \tilde{b}_l \Phi(\mathbf{K}_l) - \frac{\Delta t}{\varepsilon} \sum_{l=1}^s b_l \Psi(\mathbf{K}_l)$ .

Note that, using the above relaxation scheme neither linear algebraic equation nor nonlinear source terms can arise. In addition, since the relaxation source is treated implicitly, the high order relaxation scheme is stable independently of  $\varepsilon$ , so the choice of  $\Delta t$  is based only on the usual CFL condition

$$\text{CFL} = \max_{1 \leq \nu \leq N} \left( \frac{\Delta t}{h}, A_\nu \frac{\Delta t}{\Delta x}, B_\nu \frac{\Delta t}{\Delta y}, C_\nu \frac{\Delta t}{\Delta z} \right) \leq 1, \tag{2.7}$$

where  $h$  denotes the maximum cell size,  $h = \max(\Delta x, \Delta y, \Delta z)$ .

In this paper we use the third order IMEX scheme proposed in [2], the associated double *tableau* can be represented as

0	0	0	0	0	0	0	0
$\gamma$	$\gamma$	0	0	$\gamma$	0	$\gamma$	0
$1 - \gamma$	$\gamma - 1$	$2 - 2\gamma$	0	$1 - \gamma$	0	$1 - 2\gamma$	$\gamma$
	0	$\frac{1}{2}$	$\frac{1}{2}$		0	$\frac{1}{2}$	$\frac{1}{2}$

where  $\gamma = (3 + \sqrt{3})/6$ . Other IMEX schemes of third and higher order are also discussed in [12]. It is clear that, at the limit ( $\varepsilon \rightarrow 0$ ) the time integration procedure tends to a time integration scheme of the limit equations based on the explicit scheme given by the left table.

### 3. Implementation and Numerical Examples

We present numerical results for some benchmark tests on hyperbolic equations in two and three space dimensions using our third-order relaxation scheme. We consider both scalar and systems of nonlinear equations of conservation laws. In all the computational results presented in this section, the relaxation rate  $\varepsilon$  is set to  $10^{-8}$  and the characteristic speeds  $A_\nu$ ,  $B_\nu$  and  $C_\nu$  are chosen as

$$\begin{aligned}
 A_{i+\frac{1}{2},j,k} &= \max_{U \in \{U_{i+\frac{1}{2},j,k}^-, U_{i+\frac{1}{2},j,k}^+\}} \left| \frac{\partial \mathbf{F}}{\partial U_\nu}(U) \right|, \\
 B_{i,j+\frac{1}{2},k} &= \max_{U \in \{U_{i,j+\frac{1}{2},k}^-, U_{i,j+\frac{1}{2},k}^+\}} \left| \frac{\partial \mathbf{G}}{\partial U_\nu}(U) \right|, \\
 C_{i,j,k+\frac{1}{2}} &= \max_{U \in \{U_{i,j,k+\frac{1}{2}}^-, U_{i,j,k+\frac{1}{2}}^+\}} \left| \frac{\partial \mathbf{H}}{\partial U_\nu}(U) \right|,
 \end{aligned} \tag{3.1}$$

where the values at the cell boundary point are given by

$$\begin{aligned} U_{i+\frac{1}{2},j,k}^- &= p_i(x_{i+\frac{1}{2}}, y_j, z_k; \mathbf{U}), & U_{i+\frac{1}{2},j,k}^+ &= p_{i+1}(x_{i+\frac{1}{2}}, y_j, z_k; \mathbf{U}); \\ U_{i,j+\frac{1}{2},k}^- &= p_j(x_i, y_{j+\frac{1}{2}}, z_k; \mathbf{U}), & U_{i,j+\frac{1}{2},k}^+ &= p_{j+1}(x_i, y_{j+\frac{1}{2}}, z_k; \mathbf{U}); \\ U_{i,j,k+\frac{1}{2}}^- &= p_k(x_i, y_j, z_{k+\frac{1}{2}}; \mathbf{U}), & U_{i,j,k+\frac{1}{2}}^+ &= p_{k+1}(x_i, y_j, z_{k+\frac{1}{2}}; \mathbf{U}). \end{aligned}$$

In order to avoid initial and boundary layer in (1.2), initial and boundary conditions are chosen to be consistent to the associated local equilibrium (1.5). For instance, if Dirichlet boundary condition is given,  $\mathbf{U} = \mathbf{U}_b$ , then the boundary and initial conditions for (1.2) are given by

$$\mathbf{V} = \mathbf{F}(\mathbf{U}_b), \quad \mathbf{W} = \mathbf{G}(\mathbf{U}_b), \quad \mathbf{Z} = \mathbf{H}(\mathbf{U}_b), \tag{3.2a}$$

$$\mathbf{V}_0 = \mathbf{F}(\mathbf{U}_0), \quad \mathbf{W}_0 = \mathbf{G}(\mathbf{U}_0), \quad \mathbf{Z}_0 = \mathbf{H}(\mathbf{U}_0). \tag{3.2b}$$

A simplified flow chart for the relaxation scheme used to approximate solutions to system of equations (1.1) is presented in figure 3.1. First the semilinear relaxation system of hyperbolic equations (1.2) with initial and boundary-value independent variables is transformed into an ODE initial-value problem by approximation of the spatial derivatives with the third order reconstruction (2.3) on a “dimension by dimension” basis. Starting by an initial condition, the ODE problem is integrated in time by the higher order IMEX methods (2.6). As can be seen from the figure, the relaxation solution of (1.1) is a modular algorithm into which any higher order spatial discretization scheme and any higher order ODE solver can easily be incorporated.

Note that the algorithms presented in this paper can be highly optimized for the vector computers, because they not require nonlinear solvers and contain no recursive elements. Some difficulties arise from the fact that for efficient vectorization the data should be stored continuously within long vectors rather than three-dimensional arrays.

### 3.1. Accuracy Test Problems

**Burgers’ equation.** In order to check the accuracy of our relaxation scheme, we first consider the one-dimensional inviscid Burger’s equation

$$\frac{\partial u}{\partial t} + \left(\frac{u^2}{2}\right)_x = 0, \quad x \in [0, 2\pi], \tag{3.3}$$

augmented with the smooth initial data,  $u(x, 0) = 0.5 + \sin(x)$ , and periodic boundary conditions. The relaxation system for (3.3) is constructed as in (1.2) with  $\mathbf{A} = \{A_1\}$ . We discretize the spatial domain into  $N$  gridpoints, and we choose  $A_1 = 1.5$  in all computations. Recall that the unique entropy solution of (3.3) is smooth up to the critical time  $t = 1$ . In table 3.1 we show the errors norms at the pre-shock time  $t = 0.5$  when the solution is still smooth using CFL = 0.75. The errors are measured by the difference between the pointvalues of the exact solution and the reconstructed pointvalues of the computed solution. As expected the scheme preserves the third order of accuracy.

**Inviscid gas Euler equation.** We consider the one-dimensional Euler system of inviscid gas dynamics formulated by equations (1.1), where

$$\mathbf{U} = \begin{pmatrix} \rho \\ \rho u \\ E \end{pmatrix}, \quad \mathbf{F}(\mathbf{U}) = \begin{pmatrix} \rho u \\ \rho u^2 + p \\ u(E + p) \end{pmatrix}. \tag{3.4}$$

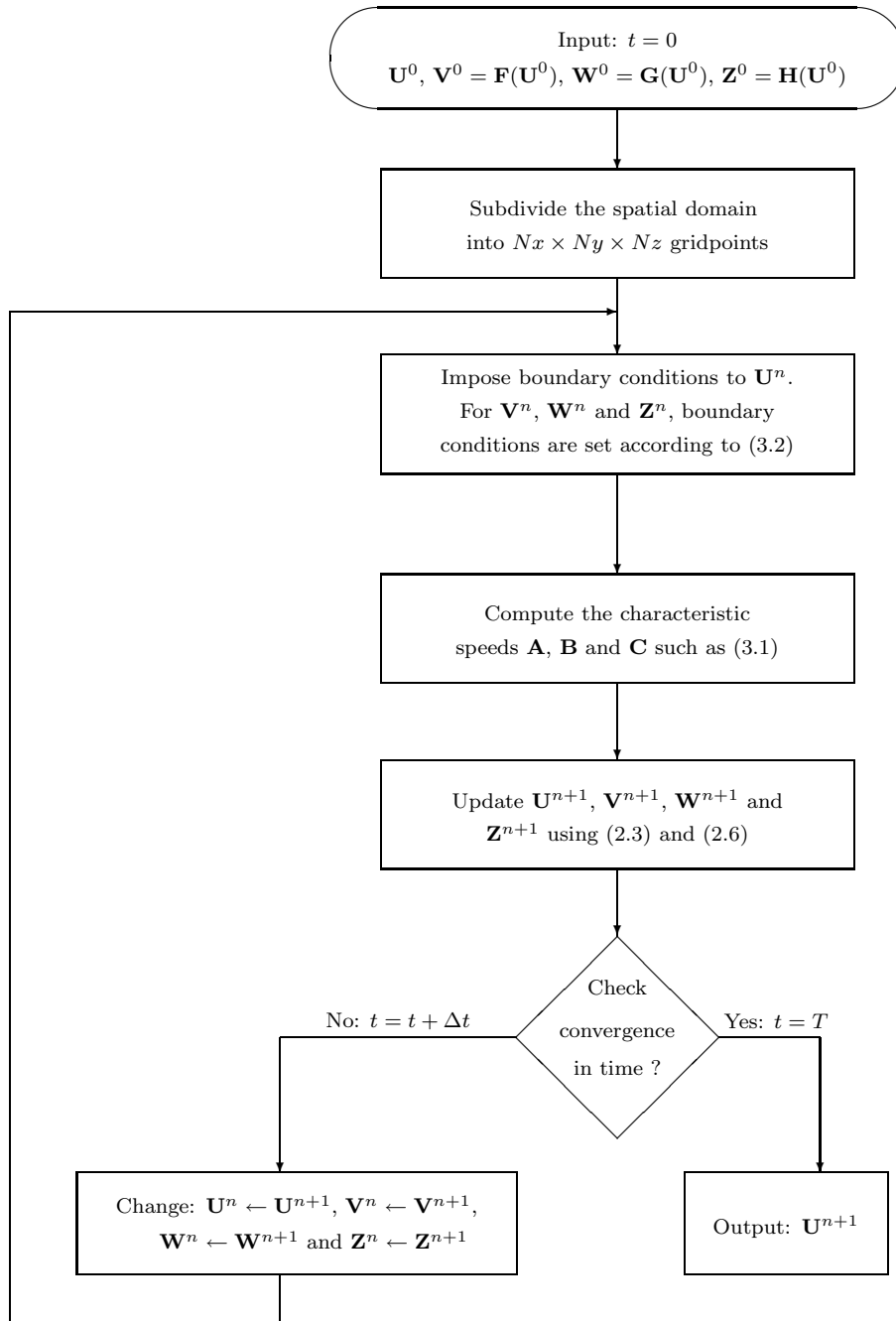


Fig. 3.1. Flow chart of relaxation schemes for the three-dimensional problem (1.1).

Here  $\rho$  is the density,  $u$  is the velocity,  $\rho u$  is the momentum,  $E$  is the energy and  $p$  is the pressure. In addition we require the equation of state  $p = (\gamma - 1)(E - \frac{1}{2}\rho u^2)$ , where the specific heats ratio  $\gamma = 1.4$  for an ideal gas. Based on the formulation (1.1), a relaxation system can be constructed as in (1.2) where  $\mathbf{A} = \text{diag}\{A_1, A_2, A_3\}$ . We used constant characteristic speeds

Table 3.1: Error-norms for the invscid Burgers' problem

$N$	$L^\infty$ -error	Rate	$L^1$ -error	Rate	$L^2$ -error	Rate
40	0.37681E-01	—	0.28977E-01	—	0.30533E-01	—
80	0.15964E-01	1.239	0.71792E-02	2.013	0.82323E-02	1.891
160	0.47363E-02	1.753	0.12559E-02	2.515	0.17511E-02	2.233
320	0.78772E-03	2.588	0.14477E-03	3.117	0.22551E-03	2.957
640	0.69819E-04	3.496	0.92831E-05	3.963	0.17196E-04	3.713

Table 3.2: Error-norms for the invscid Euler system

$N$	$L^\infty$ -error	Rate	$L^1$ -error	Rate	$L^2$ -error	Rate
40	0.30776E-00	—	0.19331E-00	—	0.25518E-00	—
80	0.94069E-01	1.710	0.52084E-01	1.892	0.73078E-01	1.804
160	0.24111E-01	1.964	0.12250E-01	2.088	0.18105E-01	2.013
320	0.53134E-02	2.182	0.21210E-02	2.530	0.35661E-02	2.344
640	0.81827E-03	2.699	0.28200E-03	2.911	0.50957E-03	2.807

$A_i$  as in [7], and we define the CFL number as in (2.7).

We solve the invscid Euler system (3.4) in space domain  $[-\pi, \pi]$  with periodic boundary conditions [14]. Initial data is obtained from the smooth exact solution

$$\mathbf{U}(x, t) = (1 + 0.2 \sin(x - t), 1 + 0.2 \sin(x - t), 3 + 0.1 \sin(x - t))^T. \quad (3.5)$$

We take  $A_1 = 0.33$ ,  $A_2 = 1$ ,  $A_3 = 2.35$  and  $\text{CFL} = 0.5$ . In table 3.2, we list the error norms for the density variable at time  $t = 1$ . Once again, the relaxation scheme preserves the third order accuracy for this nonlinear system.

### 3.2. Two-dimensional problems

**Burgers' equation.** We start by considering the invscid Burgers' equation in two space dimensions

$$\begin{aligned} \frac{\partial u}{\partial t} + \left(\frac{u^2}{2}\right)_x + \left(\frac{u^2}{2}\right)_y &= 0, \quad t > 0, \quad (x, y) \in [0, 1] \times [0, 1], \\ u(t = 0, x, y) &= \sin^2(\pi x) \sin^2(\pi y), \quad (x, y) \in [0, 1] \times [0, 1], \end{aligned} \quad (3.6)$$

augmented with periodic boundary conditions. By setting the flux functions

$$F(u) = G(u) = \frac{u^2}{2},$$

the associated relaxation system to (3.6) can be formulated as in (1.2) with  $\mathbf{A} = \text{diag}\{A\}$  and  $\mathbf{B} = \text{diag}\{B\}$ . We discretize the spatial domain uniformly into  $50 \times 50$  gridpoints and we compute the solution using  $A = 1.0$ ,  $B = 1.0$  and  $\text{CFL} = 0.75$ .

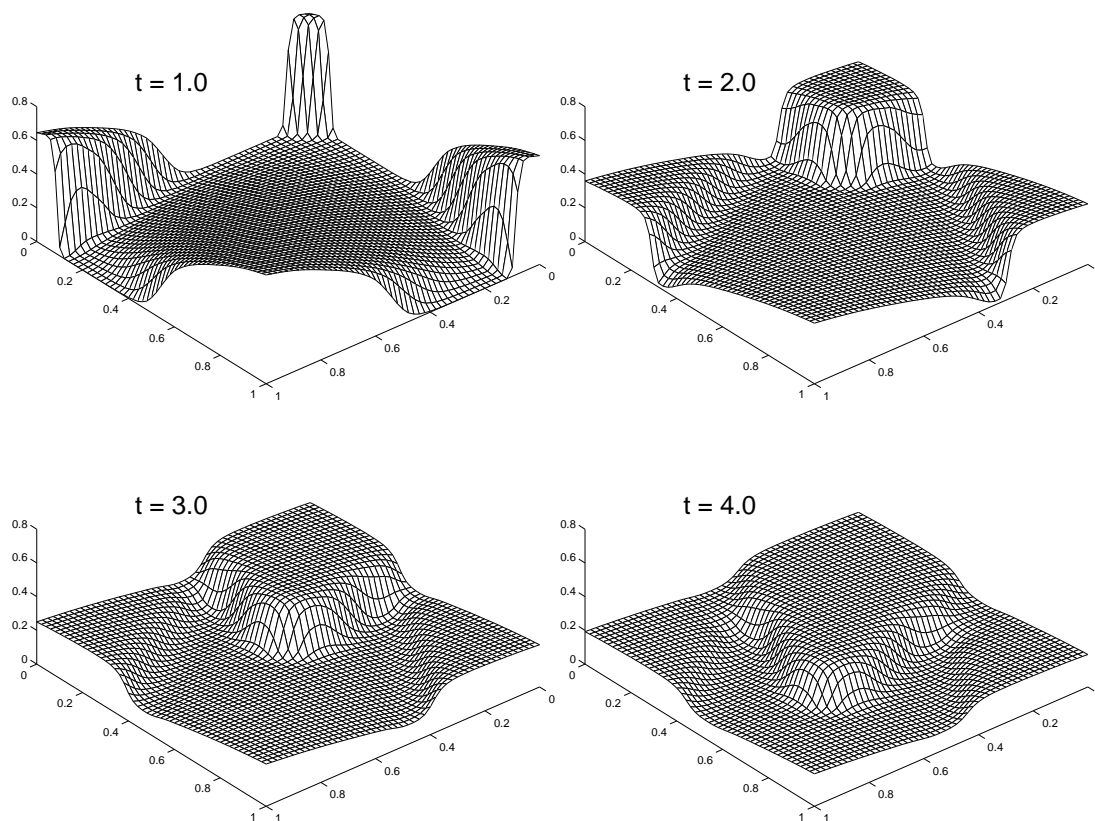


Fig. 3.2. Results for the inviscid two-dimensional Burgers' equation (3.6).

The obtained results are shown in Figure 3.2 at four different times,  $t = 1, 2, 3,$  and  $4$ . The solutions are completely free of spurious oscillations and the shocks are well resolved by the third-order relaxation scheme.

**Inviscid gas Euler equations.** The two-dimensional Euler equations for an ideal gas are given by the hyperbolic system (1.1) with

$$\mathbf{U} = \begin{pmatrix} \rho \\ \rho u \\ \rho v \\ E \end{pmatrix}, \quad \mathbf{F}(\mathbf{U}) = \begin{pmatrix} \rho u \\ \rho u^2 + p \\ \rho uv \\ u(E + p) \end{pmatrix}, \quad \mathbf{G}(\mathbf{U}) = \begin{pmatrix} \rho v \\ \rho uv \\ \rho v^2 + p \\ v(E + p) \end{pmatrix}. \quad (3.7)$$

In (3.7),  $\rho$  is the density,  $u$  is the  $x$ -velocity,  $v$  is the  $y$ -velocity,  $E = \rho e = \frac{1}{2}\rho(u^2 + v^2)$  is the total energy,  $e$  is the internal energy of the gas,  $p = (\gamma - 1)\rho e$  is the pressure, and  $\gamma = 1.4$  is the ratio of specific heats. The associated relaxation system can be formulated as (1.2), where  $\mathbf{A} = \text{diag}\{A_1, A_2, A_3, A_4\}$  and  $\mathbf{B} = \text{diag}\{B_1, B_2, B_3, B_4\}$ .

The eigenvalues of the Jacobian matrix  $\partial\mathbf{F}(\mathbf{U})/\partial\mathbf{U}$  (or  $\partial\mathbf{G}(\mathbf{U})/\partial\mathbf{U}$ ) are  $\lambda_1 = u - c$ ,  $\lambda_2 = \lambda_3 = u$  and  $\lambda_4 = u + c$  (or  $\mu_1 = v - c$ ,  $\mu_2 = \mu_3 = v$  and  $\mu_4 = v + c$ ), where  $c$  is the sound speed given by  $c^2 = \gamma p/\rho$ . These are the characteristic speeds for one-dimensional gas dynamics and are needed here only for the estimation of relaxation variables. Thus, in all our numerical tests

with equations (3.7) we used

$$A_1 = A_2 = A_3 = A_4 = \max(\sup|u - c|, \sup|u|, \sup|u + c|),$$

$$B_1 = B_2 = B_3 = B_4 = \max(\sup|v - c|, \sup|v|, \sup|v + c|).$$

**The double-Mach reflection problem.** This test example consists of the canonical double-Mach reflection problem [21]. The spatial domain  $\Omega = [0, 4] \times [0, 1]$ . The reflecting wall lies at the bottom of the computational domain starting from  $x = \frac{1}{6}$ . Initially a right-moving Mach 10 shock is positioned at  $x = \frac{1}{6}, y = 0$  and makes a  $60^\circ$  angle with the  $x$ -axis. For the bottom boundary, the exact post-shock condition is imposed for the part from  $x = 0$  to  $x = \frac{1}{6}$  and a reflective boundary condition is used for the rest. At the top boundary of the domain  $\Omega$ , the flow values are set to describe the exact motion of the Mach 10 shock. For comparison reasons, we use two different uniform meshes of  $240 \times 60$ , and  $480 \times 120$  gridpoints.

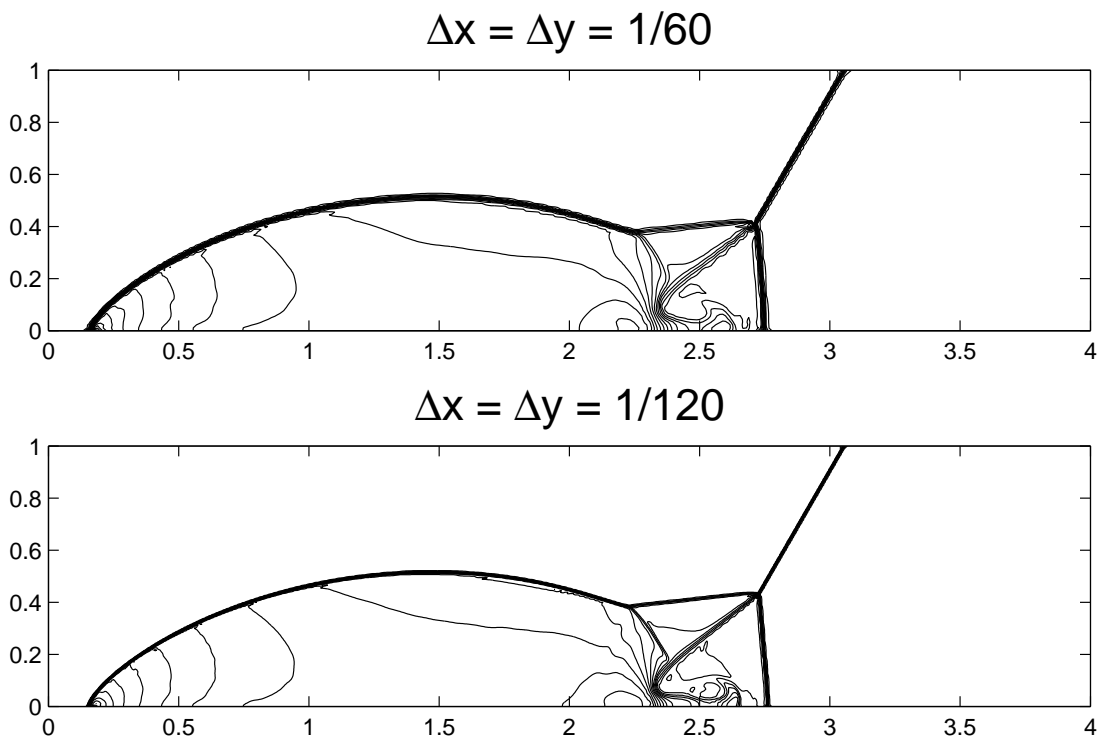


Fig. 3.3. Density contours for the double-Mach reflection problem on two meshes.

Figure 3.3 shows 30 equi-distributed contour plots of the density at time  $t = 0.2$  with  $\Delta t = 0.0005$ . We note that there is a very strong increase in resolution as the grids are refined due to the high order accuracy of the relaxation scheme. We can also see the complicated structures being captured by the new relaxation scheme. This test problem has been solved in [7] using the second order relaxation scheme. By a simple comparison between Figure 3.3 and Figure 5 in [7] we can see that our third-order scheme uses only half of the gridpoints as the second order scheme to obtain almost the same resolution. Furthermore, the resolution achieved by the new relaxation scheme agree well with most of the results obtained by central schemes, compare for example [6].

**The forward facing step problem.** This is again a standard test problem for numerical schemes in two-dimensional Euler equations of gas dynamics (3.7). The setting of the problem is the following [21]:

A right going Mach 3 uniform flow enters a wind tunnel of 1 unit wide and 3 units long. The step is 0.2 units high and is located 0.6 units from the left hand end of the tunnel. The problem is initialized by a uniform, right going Mach 3 flow. Reflective boundary conditions are applied along the walls of the tunnel and inflow and outflow boundary conditions are applied at the entrance and the exit of the tunnel, respectively.

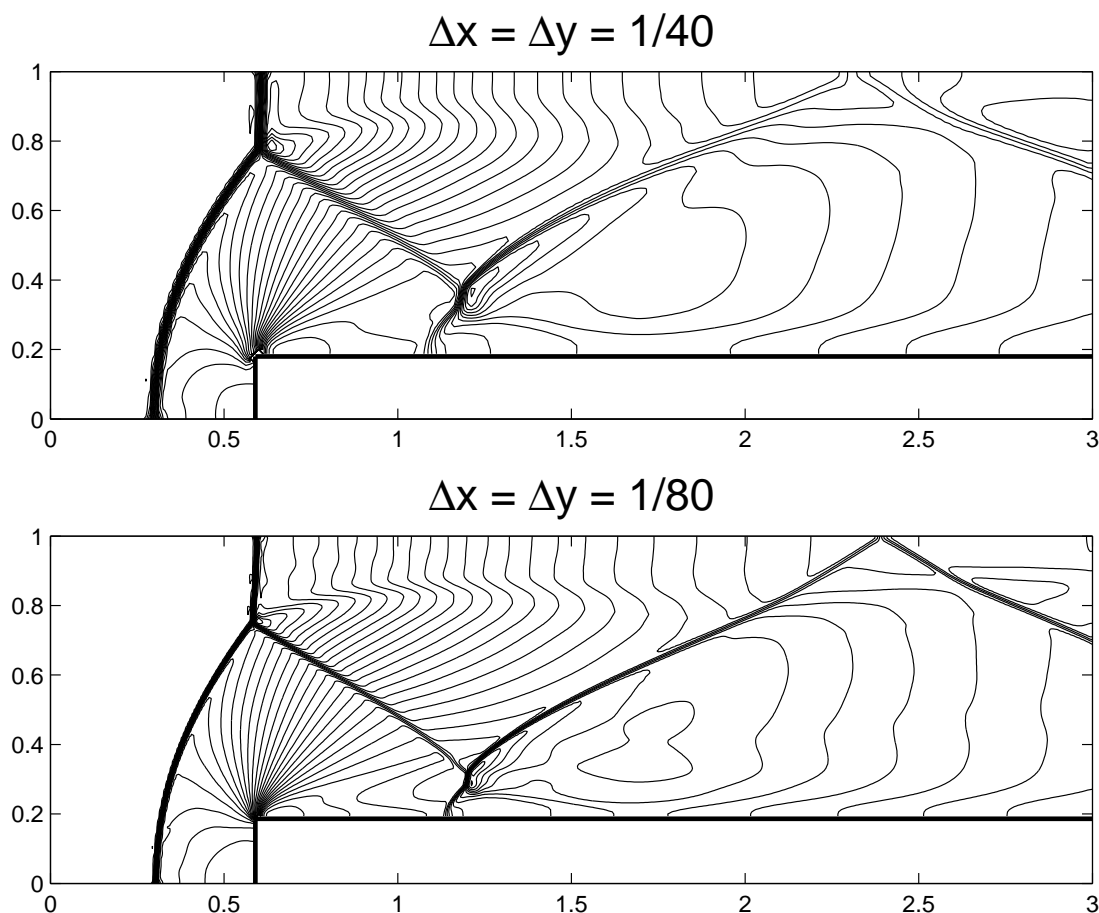


Fig. 3.4. Density contours for the forward facing step problem on two meshes.

The corner of the step is a singularity, which has to be treated carefully in numerical experiments. Unlike in [21] and many other papers, we do not modify our relaxation scheme near the corner. However, we use different grid refinements to decrease the entropy layer at the downstream bottom wall. In Figure 3.4 we show 30 equi-distributed contour plots of the density at time  $t = 4.0$  using two different uniform meshes of  $120 \times 40$ , and  $240 \times 80$  gridpoints. We can clearly see that the resolution in the solution improves and the artifacts caused by the corner decrease as long as the gridpoints on the mesh increase.

**3.3. Three-dimensional problems**

**Linear advection problem.** We consider a three-dimensional linear advection problem introduced and carefully studied in [9]. The deformation flow in this problem is obtained by superimposing deformation in  $x$ - $y$  plane with deformation in the  $x$ - $z$  plane. The problem statement is

$$\frac{\partial u}{\partial t} + v_1 \frac{\partial u}{\partial x} + v_2 \frac{\partial u}{\partial y} + v_3 \frac{\partial u}{\partial z} = 0, \quad t \in (0, T], \quad (x, y, z) \in [0, 1]^3, \quad (3.8)$$

where the velocities are given by

$$\begin{aligned} v_1(x, y, z) &= 2 \sin^2(\pi x) \sin(2\pi y) \sin(2\pi z)g(t), \\ v_2(x, y, z) &= -\sin(2\pi x) \sin^2(\pi y) \sin(2\pi z)g(t), \\ v_3(x, y, z) &= -\sin(2\pi x) \sin(2\pi y) \sin^2(\pi z)g(t). \end{aligned} \quad (3.9)$$

The function  $g(t)$  is used to introduce time dependence in the flow domain and is defined as  $g(t) = \cos(\pi t/T)$ ,  $t \in (0, T]$ . As reported in [9], the flow slows down and reverses direction in such a way that initial condition should be recovered at time  $T$  (*i.e.*  $u(0, x, y, z) = u(T, x, y, z)$ ). This is a very useful test example since the analytical solution at time  $T$  is known even though the flow structure becomes complicated at this time. Here, we use  $T = 1.5$  and the discontinuous initial condition

$$u(0, x, y, z) = \begin{cases} 1, & \text{if } x < \frac{1}{2}, \\ 0, & \text{if } x \geq \frac{1}{2}. \end{cases}$$

For this initial data, the interface at  $x = \frac{1}{2}$  deforms in a fully three-dimensional way and return to its initial location at time  $t = T$ . It is easy to verify that the velocity field (3.9) is divergence free, *i.e.*

$$\frac{\partial v_1}{\partial x} + \frac{\partial v_2}{\partial y} + \frac{\partial v_3}{\partial z} = 0.$$

This condition allows us to rewrite the equation (3.8) in a conservative form as (1.1), where the flux functions are taken as  $F(u) = v_1 u$ ,  $G(u) = v_2 u$ , and  $H(u) = v_3 u$ . Therefore, the associated relaxation system to (3.8) is constructed as (1.2) with characteristic speeds given by (3.1). We discretize the flow domain in  $50 \times 50 \times 50$  uniform cubes and a  $\Delta t = 0.5 \Delta x$  is used in our computations. In Figure 3.5 we display the obtained results at times  $t = \frac{T}{8}$ ,  $t = \frac{T}{2}$  and  $t = T$ , respectively. In this figure, the surface plots of the solution are shown only on the subdomain  $[0, 1] \times [0, 1] \times [0, 1] \setminus [\frac{1}{2}, 1] \times [\frac{1}{2}, 1] \times [0, 1]$  for better insight, while the contour plots are taken by a cross section at  $z = 0.425$  as in [9].

At  $t = \frac{T}{2}$  the interface appears disconnected and at  $t = T$  the initial interface is recovered with an non avoidable smearing introduced by the full three-dimensional deformation. The results shown here agree well with those presented in [9]. We would like to comment on the method used in [9] to solve the equation (3.8). Thus, the author in [9] proposed a high resolution scheme based on upwind techniques where direct or approximate Riemann solvers are needed. In contrast, our relaxation scheme does not require any Riemann solver and gives results which are comparable to those obtained by upwinding in [9].

**Burgers' equation.** The second test example is the three-dimensional Burgers' equation

$$\frac{\partial u}{\partial t} + \left(\frac{u^2}{2}\right)_x + \left(\frac{u^2}{2}\right)_y + \left(\frac{u^2}{2}\right)_z = 0, \quad t > 0, \quad (x, y, z) \in [0, 1]^3, \quad (3.10)$$

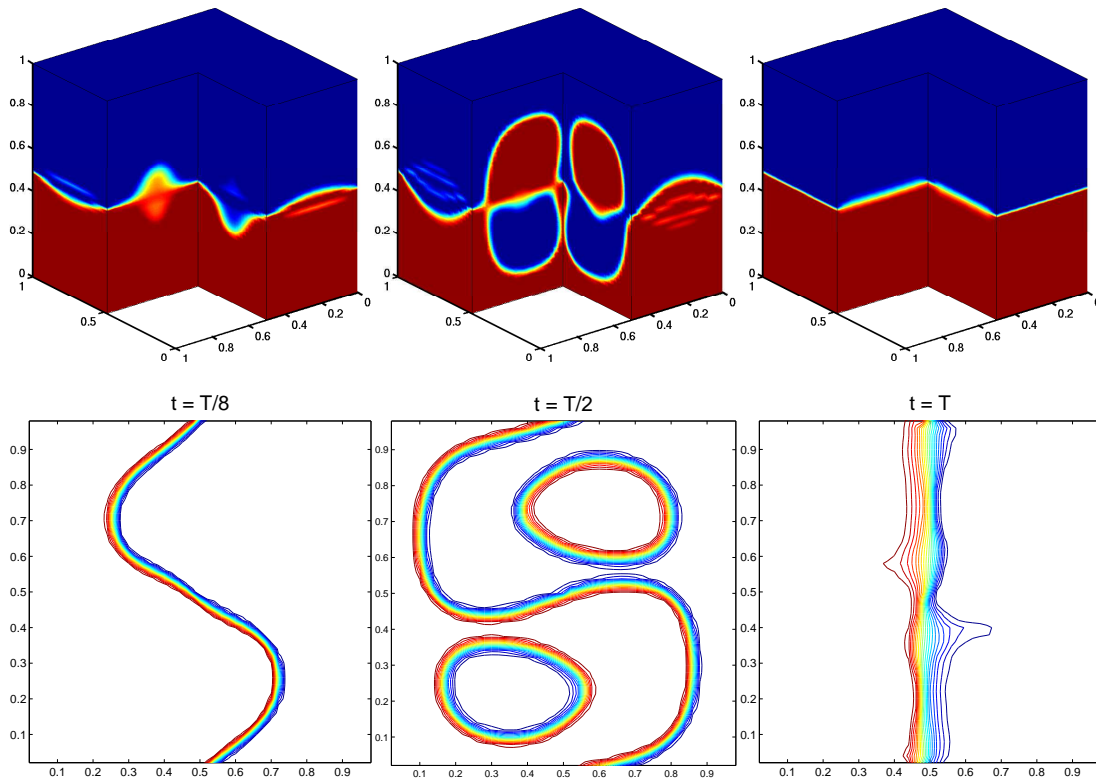


Fig. 3.5. Results for the three-dimensional advection equation (3.8).

subject to periodic boundary conditions and to the Riemann initial data

$$u(0, x, y, z) = \begin{cases} 1.5, & \text{if } x^2 + y^2 + z^2 \leq 0.01, \\ 1, & \text{otherwise.} \end{cases} \quad (3.11)$$

Note that the application of equation (3.10) to the initial data (3.11) results in a circular shock centered at the origin of the cube and moving along the main diagonal of the unit cube. The relaxation system that gives at the limit equation (3.10) is formulated as (1.2) with

$$F(u) = G(u) = H(u) = \frac{u^2}{2},$$

and characteristic speeds given by (3.1).

As in the previous example, we discretize the spatial domain uniformly into  $50 \times 50 \times 50$  gridpoints and we set  $\Delta t = 0.005$ . The obtained results are shown in Figure 3.6 at three different times  $t = 0.1$ ,  $t = 0.3$  and  $t = 0.5$ . Here in the three-dimensional plots only a part of the unit cube,  $[0, 1] \times [0, \frac{1}{2}] \times [0, \frac{1}{2}]$ , is shown. Whereas, the two-dimensional plots represents contour lines of a cross section at  $x = \frac{1}{2}$ . The third-order relaxation scheme captures accurately the evolution of the shock along the main diagonal of the computational domain without diffusing the fronts neither introducing oscillations near steep gradients.

**Riemann problem in gas dynamics.** The three-dimensional system of inviscid Euler equa-

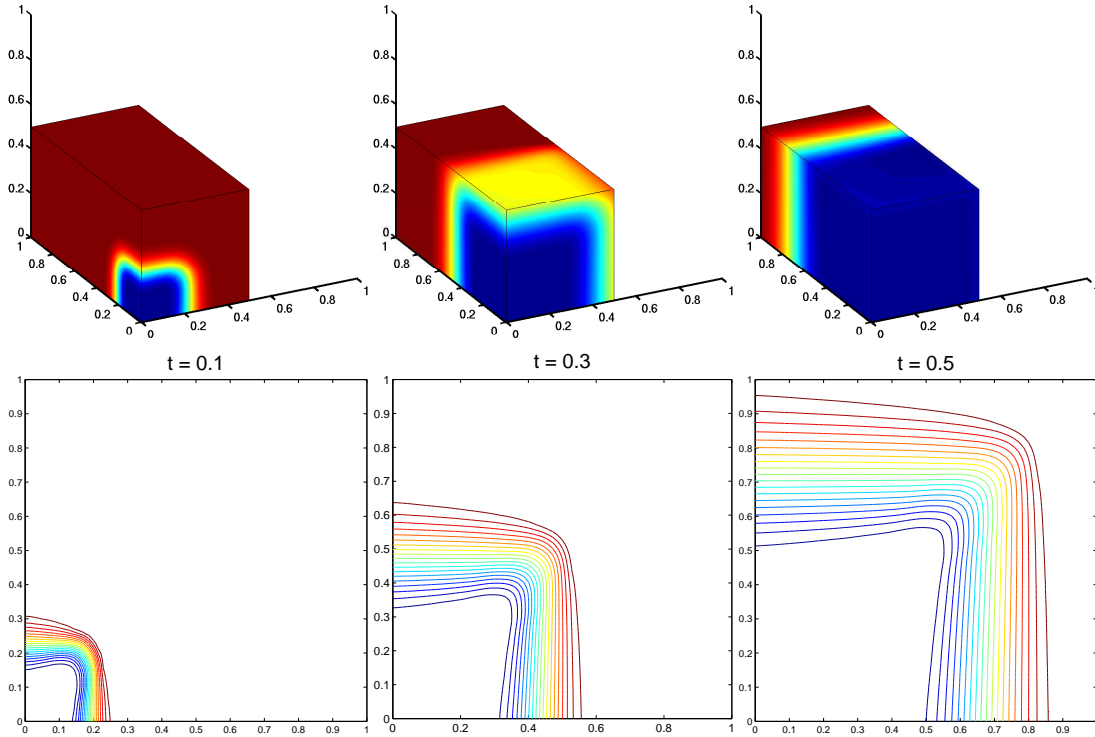


Fig. 3.6. Results for the three-dimensional Burgers' equation (3.10).

tions can be written in conservative form as (1.1) with

$$\mathbf{U} = \begin{pmatrix} \rho \\ \rho u \\ \rho v \\ \rho w \\ E \end{pmatrix}, \mathbf{F}(\mathbf{U}) = \begin{pmatrix} \rho u \\ \rho u^2 + p \\ \rho uv \\ \rho uw \\ u(E + p) \end{pmatrix}, \mathbf{G}(\mathbf{U}) = \begin{pmatrix} \rho v \\ \rho v^2 + p \\ \rho vw \\ v(E + p) \end{pmatrix}, \mathbf{H}(\mathbf{U}) = \begin{pmatrix} \rho w \\ \rho w^2 + p \\ \rho vw \\ w(E + p) \end{pmatrix}.$$

where  $\rho$ ,  $\mathbf{u} = (u, v, w)^T$ ,  $p$ , and  $E$  denote respectively the mass density, the flow velocity, the thermal pressure and the total energy. The thermal pressure and total energy are related by the equation of state  $p = (\gamma - 1)(E - \frac{\rho}{2}\mathbf{u}^2)$ .

The example we consider here, is inspired by the standard one-dimensional Sod tube shock problem [1]. Similar test example but in two dimensions was proposed in [4]. The computational domain is the unit cube  $\Omega = [0, 1] \times [0, 1] \times [0, 1]$ . To define initial conditions for this problem we first divide the domain into eight equally subcubes as:  $\Omega_1 = I_l \times I_l \times I_l$ ,  $\Omega_2 = I_l \times I_r \times I_l$ ,  $\Omega_3 = I_r \times I_l \times I_l$ ,  $\Omega_4 = I_r \times I_r \times I_l$ ,  $\Omega_5 = I_l \times I_l \times I_r$ ,  $\Omega_6 = I_l \times I_r \times I_r$ ,  $\Omega_7 = I_r \times I_l \times I_r$ ,  $\Omega_8 = I_r \times I_r \times I_r$ , with  $I_l = [0, \frac{1}{2}]$  and  $I_r = [\frac{1}{2}, 1]$ . Then, velocity is set to  $\mathbf{u} = \mathbf{0}$  in  $\Omega$ , density and pressure are alternated between the subcubes  $\Omega_i$ ,  $i = 1, \dots, 8$ , as follows

$$(\rho, p)^T(0, x, y, z) = \begin{cases} (0.1, 0.1)^T & \text{if } (x, y, z) \in \Omega_1 \cup \Omega_4 \cup \Omega_6 \cup \Omega_7, \\ (1, 1)^T & \text{if } (x, y, z) \in \Omega_2 \cup \Omega_3 \cup \Omega_5 \cup \Omega_8. \end{cases}$$

Homogeneous Neumann boundary conditions are used, and  $\Delta t = 0.001$ . The obtained results for the density variable at  $t = 0.16$  on a mesh of  $50 \times 50 \times 50$  gridpoints are illustrated in Figure

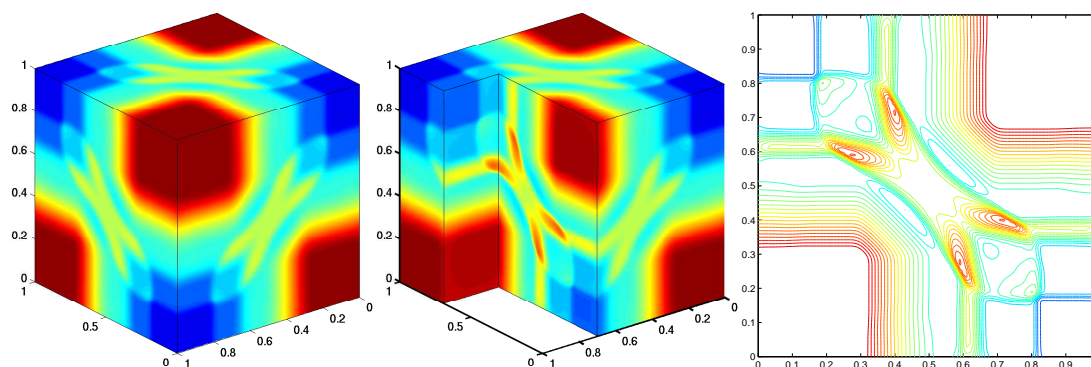


Fig. 3.7. Results for the three-dimensional inviscid Euler equations.

3.7. Here, the three-dimensional surface plots represent the distribution of density on the whole cube  $\Omega$  and on the part  $\Omega \setminus [0, \frac{2}{3}] \times [0, \frac{1}{4}] \times [0, 1]$  of the cube, while the two-dimensional plot represents the projection of density contours on the  $x$ - $y$  plane at  $z = \frac{1}{2}$ . Our relaxation scheme performs well for this test problem and high resolution of the scheme is clearly visible even on coarse mesh as the one we used.

#### 4. Concluding Remarks

Relaxation schemes of first and second order accuracy were introduced in [7]. In this paper we have reconstructed high order relaxation schemes by using WENO ideas and a class of TVD high order Runge-Kutta time integration methods. We have generalized the relaxation method for multidimensional hyperbolic systems of conservation laws. This procedure combines the attractive attributes of the two methods to yield a procedure for either scalar or system of hyperbolic equations. The new method retains all the attractive features of central schemes such as neither Riemann solvers nor characteristic decomposition are needed. Furthermore, the scheme does not require either nonlinear solution or special front tracking techniques.

The third-order relaxation method have been tested on inviscid Burgers and Euler equations in two and three space dimensions. The obtained results indicate good shock resolution with high accuracy in smooth regions and without any nonphysical oscillations near the shock areas.

#### References

- [1] D. Aregba-Driollet and R. Natalini, Discrete kinetic schemes for multidimensional systems of conservation laws, *SIAM. J. Numer. Anal.*, **37** (2000), 1973-2004.
- [2] U. Asher, S. Ruuth and R. Spiteri, Implicit-Explicit Runge-Kutta methods for time-dependent partial differential equations, *Appl. Numer. Math.*, **25** (1997), 151-167.
- [3] D. Balsara and C.W. Shu, Monotonicity preserving weighted essentially non-oscillatory schemes with increasingly high order of accuracy, *J. Comput. Phys.*, **160** (2000), 405-452.
- [4] M.K. Banda and M. Seaïd, A class of the relaxation schemes for two-dimensional Euler systems of gas dynamics, *Lect. Notes Comput. Sci.*, **2329** (2002), 930-939.
- [5] M.K. Banda and M. Seaïd, Higher-Order Relaxation Schemes for Hyperbolic Systems of Conservation Laws, *J. Numer. Math.*, **13** (2005), 171-196.

- [6] G.S. Jiang, D. Levy, C.T. Lin, S. Osher and E. Tadmor, High-resolution non-oscillatory central schemes with non-staggered grids for hyperbolic conservation laws, *SIAM J. Numer. Anal.*, **35** (1998), 2147-2168.
- [7] S. Jin and Z. Xin, The relaxation schemes for systems of conservation laws in arbitrary space dimensions, *Commun. Pur. Appl. Math.*, **48** (1995), 235-276.
- [8] C. Lattanzio and D. Serre, Convergence of a relaxation scheme for hyperbolic systems of conservation laws, *Numer. Math.*, **88** (2001), 121-134.
- [9] J. LeVeque Randall, High-resolution conservative algorithms for advection in incompressible flow, *SIAM J. Numer. Anal.*, **33** (1996), 627-665.
- [10] X.G. Li, X.J. Yu, and G.N. Chen, The third-order relaxation schemes for hyperbolic conservation laws, *J. Comput. Appl. Math.*, **138** (2002), 93-108.
- [11] R. Natalini, Convergence to equilibrium for relaxation approximations of conservation laws, *Commun. Pur. Appl. Math.*, **49** (1996), 795-823.
- [12] L. Pareschi and G. Russo, Implicit-explicit Runge-Kutta schemes for stiff systems of differential equations, *Recent Trends Numer. Anal.*, **3** (2000), 269-289.
- [13] H.J. Schroll, High resolution relaxed upwind schemes in gas dynamics, *J. Sci. Comput.*, **17** (2002), 599-607.
- [14] H.J. Schroll, Relaxed high resolution schemes for hyperbolic conservation laws, *J. Sci. Comput.*, **21** (2004), 251-279.
- [15] M. Seaïd, Nonscillatory relaxation methods for the shallow water equations in one and two space dimensions, *Int. J. Numer. Meth. Fluids*, **46** (2004), 457-484.
- [16] M. Seaïd, High-resolution relaxation scheme for the two-dimensional Riemann problems in gas dynamics, *Numer. Meth. Part. Diff. Eq.*, **22** (2006), 397-413. 2005.
- [17] C.W. Shu and S. Osher, Efficient implementation of essentially non-oscillatory shock-capturing schemes, *J. Comput. Phys.*, **77** (1988), 439-471.
- [18] H.-Z. Tang and G. Warnecke, High resolution schemes for conservation laws and convection-diffusion equations with varying time and space grids, *J. Comput. Math.*, **77** (2006), 121-140.
- [19] H.Z. Tang, T. Tang, and J.H. Wang, On numerical entropy inequalities for second order relaxed schemes, *Q. Appl. Math.*, **59** (2001), 391-399.
- [20] E Tadmor and T. Tang, Pointwise error estimates for relaxation approximations to conservation laws, *SIAM J. Numer. Anal.*, **32** (2000), 870-886.
- [21] P. Woodward and P. Colella, The numerical simulation of two-dimensional fluid flow with strong shocks, *J. Comput. Phys.*, **54** (1984), 115-173.